DD

KEK Preprint 97-243
December 1997
H

Measurements of the Photon Detection Inefficiency of Calorimeters between 185 and 505 MeV

S. Ajimura[1], T. Endo[2], T. Inagaki[3], S. Itoh[4], Y. Kuno[3], K. Maeda[2], K. Maruyama[5], T. Nakano[1], H. Okuno[6], T. Sato[3], T. Shinkawa[3], T. Suda[2], K. Sugiyama[1], T. Terasawa[7] and A. Toyofuku[2]

[1] *Department of Physics, Osaka University, Osaka 560, Japan*
[2] *Department of Physics, Tohoku University, Sendai 980, Japan*
[3] *High Energy Accelerator Research Organization (KEK), Tsukuba 305, Japan*
[4] *The Institute of Physical and Chemical Research, Wako 351-01, Japan*
[5] *Center for Nuclear Study, University of Tokyo, Tanashi, Tokyo 188, Japan*
[6] *KEK, Tanashi-branch, Tanashi, Tokyo 188, Japan*
[7] *Laboratory of Nuclear Science, Tohoku University, Sendai 982, Japan*

Abstract

The detection inefficiencies for photons of total-absorption-type electromagnetic calorimeters, an undoped CsI crystal counter and a lead-scintillator sandwich counter, have been measured at photon energies (E_γ) between 185 and 505 MeV with the tagged photon beam from the INS-ES. The effect of punch-through is estimated by an EGS calculation. The other one, the photonuclear interaction effect, is examined after the interaction is identified by neutron signals observed with liquid scintillation counters surrounding the sample calorimeter. The inefficiency due to the photonuclear interaction in the case of the CsI calorimeter at 1-MeV threshold is found to be $10^{-5} - 10^{-6}$ and shows a monotonous decrease with E_γ. The detection inefficiency of the sandwich calorimeter is found to be dominated by the sampling effect after photonuclear interactions.

Submitted to Nucl. Instrum. Meth. A.

** From April 1, 1997, **High Energy Accelerator Research Organization (KEK)** was newly established. The new organization is restructured of three reseach institutes, National Laboratory for High Energy Physics (KEK), Institues of Nuclear Study (INS), Univ. of Tokyo and Meson Science Laboratory, Faculty of Science, Univ. of Tokyo.*

High Energy Accelerator Research Organization (KEK), 1997

KEK Reports are available from:

Information Resources Division
High Energy Accelerator Research Organization (KEK)
1-1 Oho, Tsukuba-shi
Ibaraki-ken, 305
JAPAN

Phone: 0298-64-5137
Fax: 0298-64-4604
Cable: KEK OHO
E-mail: Library@kekvax.kek.jp (Internet Address)
Internet: http://www.kek.jp

1 Introduction

It is crucial to know the detection inefficiency of calorimeter for photons in some high-energy experiments such as the measurement of the $K_L^0 \to \pi^0\nu\overline{\nu}$ decay branching ratio [1]. In the above experiment the decay will be identified as $\pi^0 + nothing$, where *nothing* means no emission of visible particles. So, the association of other particles should be detected with a high detection efficiency.

This paper describes the first dedicated measurement of the detection inefficiency for photons, while those for charged particles were reported elsewhere [2].

Three processes are regarded as the source of the inefficiency for photons in the case of a total-absorption-type electromagnetic calorimeter. The first one is the punch-through that a photon penetrates through the calorimeter without any interactions. Since the electromagnetic-cascade-shower process is a dominant process for photons, the probability of the punch-through could be evaluated with the electromagnetic cascade shower code, EGS [3]. However, since the punch-through for a total-absorption-type calorimeter is a tiny effect compared to most of phenomena well simulated by the EGS, the validity of the estimation has to be experimentally examined.

The second source is photonuclear interactions. When a photonuclear interaction takes place in the calorimeter in advance of an electromagnetic cascade shower and secondary particles produced in the interaction do not generate any large signals above the detection threshold, it causes the detection inefficiency. In this case the secondaries may be neutrons or charged particles with low energies below the detection threshold. A numerical evaluation of the detection inefficiency due to the photonuclear interaction is rather difficult than that due to the punch-through. The total photonuclear cross section for calorimeter materials can be calculated from the experimental data which have been measured at various energies for several nuclei, and then the ratio of the strength of photonuclear and electromagnetic interactions can be estimated with little ambiguity. However, it is no feasible to know about secondaries after the photonuclear interaction together with the calorimeter response for these particles. Since no realistic simulation code exists, the detection inefficiency due to the photonuclear interaction should be ex-

perimentally estimated.

The last one is the sampling effect which arises in the case of a sampling calorimeter such as a lead-scintillator sandwich counter. The sampling effect could be divided into two according to the type of the interaction process. One is the electromagnetic cascade shower process such as a multi-step Compton scattering where all tracks of secondary electrons are confined within the converter (non-active). This can be also estimated from an EGS calculation. The other is a photonuclear interaction followed by the absorption of the secondaries in the converter, and the effect can not be reliably evaluated by any calculations.

In the photon energy (E_γ) region from a few MeV to GeV, the photonuclear interaction cross-section drastically changes its behavior in contrast with that of the electromagnetic cascade shower process. Around 20 MeV the photonuclear interaction cross section is as large as a few percent of that of the electromagnetic cascade shower process due to the giant dipole resonance, and then it rapidly decreases with E_γ. However, below the pion-production threshold ($E_\gamma < 140$ MeV) there are a lot of cross-section data of the $\sigma(\gamma, n's)$ reactions and then the detection inefficiency can be estimated using the data [4] with a small correction for the emission of visible particles. It is because emissions of charged particles, protons, d or α are suppressed by the Coulomb barrier. On the other hand above the pion threshold ($E_\gamma > 140$ MeV) the dominant process is the pion production. The cross section rises due to the excitation of the nucleon resonances up to 0.1 % level of the electromagnetic-cascade-shower cross-section. Since the produced pions are visible in the calorimeter and many of recoil protons have energies high enough to penetrate the Coulomb barrier, the detection inefficiency would be largely reduced from the value simply calculated from the cross-section ratio between the photonuclear and electromagnetic cascade shower processes. This effect cannot be easily estimated without knowing the details about secondaries. The detection inefficiency must be evaluated by an experiment especially in this region. Since the number of visible particles produced by an interaction increases and the detection inefficiency decreases with energy, the first nucleon resonance (Δ resonance) region is selected for the present measurement as a most important region.

For the measurement we use a tagged photon beam: photons are produced via the bremsstrahlung process in which recoil electrons are measured with a magnet spectrometer. After several tests prior to the present experiment it is found impossible to get a high-purity beam (the tagged photon beam with a high tagging efficiency) enough to directly measure the detection inefficiency at a 10^{-5} level. For the direct measurement it is required that the photon exists just at the calorimeter for each tagging signal with a probability higher than the detection efficiency which we want to measure. However, unfortunately in the present tagging method there are several processes which cause a large miss tagging (a swing-and-miss) rate as illustrated in Figures 1: (a) low-energy beam electrons as a halo, (b) a two-step interaction in the radiator to produce e^+e^- which are swept away by an analyzer magnet, (c) the tagged photon emitted in a large angle outside the acceptance of the sample calorimeter due to a Coulomb scattering of the incident electron in the radiator, *etc.* It is hard to reduce at once these processes causing the miss tagging: for examples, a thicker radiator is required against (a) but it enhances (b) and (c).

In the present experiment a large volume of liquid scintillator surrounds the sample calorimeter. At first most of the miss tagging can be reduced by requiring a signal in the liquid scintillator which coincides with the tagging-signal. Moreover, the liquid scintillator can select neutron signals and this will be used for an identification of a photonuclear interaction in the calorimeter. Since a large number of neutrons (more than ten) are expected to emerge after a photonuclear interaction, at-least-one of them can be efficiently detected with the liquid scintillator of a large volume. The identification of the photonuclear interaction could be checked over-all by a comparison with the existing data of the total photonuclear interaction cross-section.

2 Experimental Method

The experiment has been carried out with the photon tagging system [5] at the electron synchrotron of the Institute for Nuclear Study (INS-ES). The setup is essentially divided into two: the tagging and sample calorimeter systems, as shown in Figure 2. Incident

electrons are extracted from the INS-ES at the peak energy of 600 MeV and hit a radiator of an aluminum foil of 0.35 mm thick (3.9×10^{-3} radiation-length) and produce bremsstrahlung photons. Since the INS-ES is operated with a resonance excitation, the beam energy sinusoidally varies by about 5 % in a beam duration for a 10 % duty factor. The energy variation is compensated by synchronously adjusting the field of the beam-line magnets to keep the beam trajectory at the right position [6] and the incident electron energy for each photon can be calculated in an off-line analysis from information of the beam timing with respect to the excitation of the synchrotron magnets.

Scattered electrons after bremsstrahlung are bent by an analyzer magnet and detected with two sets of hodoscopes consisting of 32 and 8 scintillation counters. The former 32 counters (tagging counters) are placed along the focal line of the analyzer magnet with respect to the radiator and cover a momentum range of 95-415 MeV/c with an acceptance of ± 5 MeV/c for each counter. Each of the 8 scintillation counters is a backing counter for every four-tagging counters. A coincidence signal between a tagging counter and a corresponding backing counter is called 'tag-signal'. Since the recoil energy to the radiator atoms is negligibly small, the photon energy E_γ is given as $E_\gamma = E_0 - E_e$ in a good approximation, where E_0 and E_e are the energies of the incident and scattered electrons, respectively. E_γ is determined (tagged) by a 10-MeV step over the range from 185 to 505 MeV. Details of the INS-ES tagging system were reported in the references [5] and [6].

Two types of calorimeters are prepared as the sample calorimeter to study the detection inefficiency for photons. One is an undoped-CsI -crystal calorimeter of 30-cm thick. It consists of ten blocks (one center block and nine side blocks) which are tightly packed as shown in Figure 3. The light output is directly read from the back (downstream) by a $1\frac{1}{8}$-inch diameter photomultiplier tube (PMT) for each side-block and a 2-inch PMT for the center block. The lateral radius of the whole assembly is 7.4 cm and it is about twice the Morier-Radius. The other is a lead-scintillator sandwich calorimeter with 41 layers of 6-mm thick plastic scintillator plates intervened by 2-mm thick lead plates as shown in Figure 4. The light is read from the sides of hexagon by six 2-inch PMT's via six wave-length-shifter bars. The sandwich counter is contained in a stainless-steel pipe

of 2-mm thick.

Twelve modules of the liquid scintillator (LS) surround the sample calorimeter. Four modules on each of the up-, right- and left-side direct the sample calorimeter as shown in Figures 2 and 5. Each module of 10-l liquid scintillator (NE213) in an aluminum vessel of 200-mm in diameter and 330-mm in length is viewed by a 5-inch PMT. Three long-plastic-scintillators (PV) of 10-mm thick are placed to detect charged particles on the sample side of the liquid scintillator modules. Each one covers four LS modules on each side of the sample calorimeter and the PV signal is read from both ends.

The sample calorimeter system is placed at the distance of 4-m from the radiator. Materials between the radiator and the sample calorimeter are 1.5-m air of 10^{-2} torr, a Mylar sheet of 250-μm thick and 2.5-m air of an atmospheric pressure.

In order to reduce the miss-tagging rate various veto counters are installed in the tagging system as indicated in Figure 2. Although the miss tagging can not be eliminated down to the level of 10^{-5}, it is very important to reduce it as low as possible. This can be clearly understood when we consider the accidental coincidence between a tag-signal and a LS-signal which would seriously suffer the detection inefficiency measurement. The low rate of miss tagging means that a tag-signal associates a photon with high probability. The tag-signal, even which accidentally associates a background LS signal, hardly gives a zero-signal (of the sample calorimeter) which contributes to the inefficiency. The accidental coincidences only slightly change the normalization number that is a denominator in the evaluation of the inefficiency. The low rate of miss tagging is especially important, when we use a large volume liquid scintillator.

Two hole counters (HU and HD) of plastic scintillator sandwich the radiator to reject the beam halo. A long plastic scintillator (E^+) is set in the magnet on the other side of the tagging counters with respect to the beam axis. These HU, HD and E^+ are installed in the vacuum chamber. A pair of long plastic scintillation counters (MU and MD) which cover the tagging counter region are set at the exit of the magnet to define the vertical acceptance of the tagging counters as 3 cm instead of their size of 5 cm (the gap of the magnet is also 5 cm). In front of the beam dump for 600 MeV electrons a plastic scintillation counter (BV) of 10-cm squared is placed. A pair of hole counters which are

made of undoped CsI are placed along the photon beam axis. The dimensions of the upstream (AU) and downstream (AD) counters are 6 (thick) × 10 (high) × 12(wide) cm^3 with a hole of 3-cm diameter and 5 (thick) × 10 (high) × 20(wide) cm^3 with a hole of 2-cm diameter, respectively. The AD is placed at a position 37-cm upstream from the face of the sample calorimeter in the case of the ordinary position of the sample calorimeter and AU is placed 1.5-m upstream from AD.

Figure 6 shows an electronics block-diagram. The PMT outputs of the veto counters, LS and PV are fed to ADC and the signals of the sample calorimeter are fed to double ADC's (LeCroy 2249A) of high and low ranges. The ratio of the ranges is 1:10. The PMT gains of the sample calorimeters are adjusted to be 1.5-ch/MeV (for CsI) and 1-ch/MeV (for sandwich) for the high-range ADC by using an electron beam of 600 MeV. The electron beam with the energy spread less than 1 % and the spot size of 3-mm in diameter can be provided by removing the radiator and turning off the excitation of the analyzer magnet. The PMT gain of the LS and the PSD (Pulse-Shape-Discriminator, CAMBERA-2160) equipped to every two LS modules are calibrated several times during the experiment by using checking sources of ^{60}Co and Am/Be. The threshold of the discriminator for the LS is 0.1-MeV equivalent to electrons. The time differences of all PMT signals from the trigger signal are measured by TDC.

Except for special check-runs we have taken data with the trigger which only requires the tag-signal with anti-coincidences of all veto-counters. The accelerator has been stably operated during the data acquisition. The rates of the incident electrons and the tag- and LS-signals are around 1.5k/spill (300kHz), 5/spill (1kHz) and 3/spill (0.6kHz), respectively. The values shown in the parentheses are the instantaneous rates for a duty-factor of 10 % which has been carefully kept in the operation.

3 Results for the CsI Calorimeter

The photon energy, E_γ, is determined by the hit tagging-counter number with a correction for the change of the incident electron energy with the extraction timing. The gain of the sample calorimeters is finally calibrated by the tagged photon beam in an off-line

analysis. Since a temperature dependence of the gain of the CsI is observed, the gain calibration is performed several times using real data to compensate the variation. The gain of the sandwich calorimeter is also calibrated with tagged photons. We call these energy calibrated ADC values as $E_{\rm CsI}$ and $E_{\rm Sand}$. The $E_{\rm CsI}$ and $E_{\rm Sand}$ correspond to the deposit energy in the CsI and that of the plastic scintillator in which their peaks are normalized to E_γ, respectively.

A lego plot of E_γ vs $E_{\rm CsI}$ in Figure 7 shows a good correlation between E_γ and $E_{\rm CsI}$ and a $1/E_\gamma$ spectrum which is consistent with bremsstrahlung. Figure 8 shows a tagging-counter-number dependence of the miss tagging rate, $N(E_{CsI} < 1\text{MeV})/N(all)$, where $N(E_{CsI} < 1\text{MeV})$ is the number of events whose $E_{\rm CsI}$ are less than 1 MeV and $N(all)$ the total count of every tagging counter. The miss tagging rate increases at both ends, which indicates that the contamination from secondary electrons with the momenta outside the tagging counter acceptance is large. Anyhow the miss tagging rate is suppressed to be 2 - 0.3 %.

Analysis of Tail Region

A typical $E_{\rm CsI}$ distribution of the selected events at E_γ=250±20 MeV is shown in Figure 9. In order to study the data with low deposit-energy in the CsI we select the events in the region of $E_{\rm CsI}/E_\gamma$<0.45 (tail events). The typical $E_{\rm CsI}$ distribution of the selected events at E_γ=250±20 MeV is shown in Figure 9. The CsI-TDC data (for the central block, $t_{\rm CsI}$) of the tail events suggest the existence of two components as shown in Figures 10(a) and 10(b), which are a two-dimensional plot of $t_{\rm CsI}$ and $E_{\rm CsI}$ and its distribution projected onto the $t_{\rm CsI}$ axis, respectively. Since the PV which is placed in front of the LS can measure the hit position along the beam axis and is sensitive to photons and neutrons slightly as well as to charged particles, we select the events with a signal in PV and evaluate the hit position using the time difference between the up- and down-stream PMT's. $t_{\rm CsI}$ and the hit position on the PV show correlations as shown in Figures 11(a) and 11(b). Figure 11(a) is a plot of all sample events including the peak region and 11(b) is that of the tail events. Although a single cluster is observed for the all sample events dominated by the events in the peak region, two clusters of events are seen in the tail region: late-upstream and early-downstream.

The two-cluster structure can be explained as follows by using Figures 12. After photons incident upon a calorimeter, they start to be converted into electromagnetic cascade showers from various positions as shown in Figure 12(a). The deposit energy depends on the conversion depth in the calorimeter (shower-start) as schematically depicted in Figure 12(b). Therefore, as far as the cascade shower concern, the events in the tail region are those converted at a deep position beyond B in Figure 12(a) where the incident photon penetrates almost through the calorimeter (punch-through). On the other hand the deposit-energy can be also reduced by a photonuclear interaction. Since the rate of the photonuclear interaction is proportional to the number of incident photons which decreases with the depth, most events with photonuclear interactions appear in the upstream position of the calorimeter as shown in Figure 12(c). Consequently, two components in different positions are to be observed in the tail region. In the case of the CsI calorimeter, the light velocity in CsI is low due to the high refractive index, and a time difference appears for different positions of the light-source as shown in Figure 12(d). This is the reason why we see two clusters in Figure 11(b). The early-downstream cluster corresponds to the electromagnetic cascade shower process almost near to the punch-through, and the late-upstream one to the photonuclear interaction.

Punch Through

According to the speculation the early-cluster events with -4ns$<t_{\rm CsI}<$-1ns are compared to those obtained from an EGS calculation as shown in Figure 13. The data are well reproduced by the calculation which is normalized in the number of incident photons. It should be reminded that the real event is selected by using $t_{\rm CsI}$ in which the deposit energy is required to be above the threshold (2-MeV electron equivalent). On the other hand the calculated histogram shows an enhancement below 1-MeV which corresponds to the punch-through. The agreement above the threshold justifies our method to use the EGS in the estimation of the punch-through. Table 1 shows the detection inefficiency due to the punch-through thus obtained from an EGS calculation.

Detection Inefficiency due to the Photonuclear Interaction

The late cluster may include the photonuclear interaction events. Figures 14 show time spectra measured with the PSD modules for the LS ($t_{\rm PSD}$), where 14(a) is the

$t_{\rm PSD}$ spectrum for the monitor data of the γ rays and neutrons from an Am/Be source, 14(b) for the events in the peak region, and 14(c) and 14(d) for the events with -1ns$<t_{\rm CsI}<$2ns and -4ns$<t_{\rm CsI}<$-1ns in the tail region, respectively. A clear enhancement is observed in Figure 14(c) at a large $t_{\rm PSD}$ where neutron signals are expected to exist according to the monitor data using the Am/Be source. The late cluster largely contains neutron signals which are generated by photonuclear interactions. The early cluster which has been explained as an electromagnetic cascade shower effect near to the punch-through can be surely eliminated by selecting the large $t_{\rm PSD}$ events as shown in Figure 14(c). Thus, we can conclude that the photonuclear interaction can be cleanly tagged by the neutron call in the tail region. Another important point is that the neutron call reduces the miss tagging rate down to the level of accidental coincidence.

In order to require a tight neutron call we place criteria on the PSD, ADC ($a_{\rm LS}$) and TDC ($t_{\rm LS}$) values from the LS as 15ns$<t_{\rm PSD}<$50ns, 0.1MeV$<a_{\rm LS}<$30MeV and $t_{\rm LS}<$30ns, where $a_{\rm LS}$ is the deposit energy on the LS in a scale for γ rays calibrated with ^{60}Co.

The detection inefficiency of the CsI calorimeter due to the photonuclear interaction ($DINEF$) can be calculated as a ratio between the number of the events of $E_{\rm CsI}<$1 MeV with the neutron call ($N(E_{CsI} < 1MeV : n)$) and that of all events ($N(all)$) using an equation of

$$DINEF = \frac{N(E_{CsI} < 1MeV : n)}{N(all)} \cdot \frac{1}{\eta_{\rm LS}}, \qquad (1)$$

where $\eta_{\rm LS}$ is the neutron detection efficiency of the LS.

$N(E_{CsI} < 1MeV : n)$ is estimated from the $E_{\rm CsI}$ distributions with the neutron call, which are shown in Figures 15, as a mean value of the content of the bin of $E_{\rm CsI}<$10MeV for each of eight E_γ bins. Figure 16 shows the $E_{\rm CsI}$ distribution below 10 MeV summed up over the entire E_γ region as a check. It is consistent to be flat with $E_{\rm CsI}$ within the statistical error. The mean value for $E_{\rm CsI}<$10MeV is indicated by the solid line.

$N(all)$ is the total number of events including the peak region in each E_γ bin without the neutron call.

The neutron detection efficiency of the LS, $\eta_{\rm LS}$, is estimated from the multiplicity ($m_{\rm LS}$) distribution of neutron hits. Since the events of zero-multiplicity that corresponds

to the no-use of the LS can not be directly counted without noise, the probability of the zero-multiplicity is estimated from a Poisson distribution reproducing the data of $m_{\rm LS}\geq 1$. The Poisson distribution reproduces well the data at every E_γ bin as shown in Figures 17, in which the whole data in the tail region ($E_{\rm CsI}/E_\gamma<0.45$) are used. Then, the detection efficiency is given by $1 - exp(-\mu)$, where the μ is the mean-value of the Poisson distribution. An E_γ dependence of the μ is shown in Figure 18.

The detection inefficiency of the CsI calorimeter due to the photonuclear interaction , $DINEF$, is listed in Table 1 and shown in Figure 19. The detection inefficiency monotonically decreases with photon energy from 1×10^{-5} to 1×10^{-6} in the range 185-505 MeV.

4 Checks of the Results for the CsI Calorimeter

Neutron Detection Efficiency of the LS

The overall neutron detection efficiency, $\eta_{\rm LS}$, given in Equation 1 is estimated using the whole data in the tail region ($E_{\rm CsI}/E_\gamma<0.45$). It is implicitly assumed that the efficiency does not depend on $E_{\rm CsI}/E_\gamma$, but in fact the $\eta_{\rm LS}$ (and μ) may depend on the process such as the multiplicity of neutrons and their energies. If the process largely changes with the deposit energy in the CsI, the μ may vary with $E_{\rm CsI}/E_\gamma$. We examine the variation of the μ with $E_{\rm CsI}/E_\gamma$, and find no significant dependence on $E_{\rm CsI}/E_\gamma$ except for a systematic E_γ difference, which is already folded in the estimation of the neutron detection efficiency, as shown in Figure 20.

As an over-all check we take a ratio between the number of the events with neutron signals in the tail region and the total number of events. The E_γ dependence of the ratio divided by the $\eta_{\rm LS}$ is shown in Figure 21. The curve represents the ratio between the cross sections of the photonuclear interaction and the electromagnetic cascade shower process, where we estimate the photonuclear interaction cross section by using the data of Be target [7] with an assumption of the A^1 dependence (where A is the mass-number of the target nucleus) and the cross section of the electromagnetic cascade shower process is calculated with EGS. The data and the curve show a good resemblance typical in the bump due to

the Δ resonance, and it indicates us a good identification of the photonuclear interaction. For an explicit comparison between the data and the calculation we should know the fraction which may arise due to the partial selection of the tail region ($E_{\rm CsI}/E_\gamma$<0.45) and its E_γ dependence.

For one-third of the running time we took data at a different position of the CsI calorimeter relative to the LS (30-cm downstream of the normal position shown in Figure 4). If the reactions were different in between the zero and the other tail-regions, for examples, the main contribution for $E_{\rm CsI}$<1MeV were a one-step violent reaction $A(\gamma, n's)A'_{gs}$ not like the evaporation in the tail region, the geometrical acceptance for those neutrons (the formers go more forward than the latters) might change by changing the CsI position relative to the LS. No significant difference between the two runs is observed in the final values of the detection inefficiency, and we combine them in the analysis.

Accidental Background

The accidental rate between the tagging and neutron signals is given as $\tau \cdot \dot{\rm N}_{\rm LS} \cdot \dot{\rm N}_{\rm Tag}$, where τ is the time window for neutron signals, $\dot{\rm N}_{\rm LS}$ the rate of neutron signals and $\dot{\rm N}_{\rm Tag}$ the rate of all tagging counters. Since the signal rate is almost equal to $\dot{\rm N}_{\rm Tag}$, the contamination by the accidental coincidence (noise-to-signal ratio) is expressed as $\tau \cdot \dot{\rm N}_{\rm LS}$. Taking the values of the τ = 30 ns and $\dot{\rm N}_{\rm LS} \leq$ 6 Hz (the instantaneous rate of LS is about 0.6 kHz for the discriminator threshold of 0.1 MeV and a fraction of neutron signals is less than 0.01), the contamination is less than 1.8×10^{-7}. However, another factor of 0.01 exists thanks to the small miss tagging rate, because most of tag-signals associates the photon and it does not contribute the detection inefficiency. Then the accidental background is expected to be less than 1.8×10^{-9}. It is negligibly small for the present evaluation of the detection inefficiency, even if we consider the maximum change of the duty factor from 10 to 3% (the instantaneous rate would be increased by a factor of three). The probability of an accidental overlap to the signal of zero deposit-energy, which makes the detection inefficiency under estimate, is also negligibly small, because the CsI-ADC gate time of 100 ns is already very short against the rate of CsI which is estimated to be a few kHz above the threshold of 1 MeV based on the $1/E_\gamma$ spectrum.

5 Results for the Sandwich Calorimeter

Based on the study of the CsI calorimeter, the punch-through effect for the sandwich calorimeter is estimated from an EGS calculation. The sampling effect due to the electromagnetic cascade shower are included in the calculation, because the events with a none-or-small deposit-energy ($E_{\rm Sand}$<1 MeV) are selected in the calculation regardless of process as those which contribute to the detection inefficiency. The result is listed in Table 2. The detection inefficiency due to the photonuclear interaction of the sandwich calorimeter is obtained from the events with neutrons in the same way as that of the CsI calorimeter.

Figures 22 show the $E_{\rm Sand}$ distributions for the events with neutron signals in the various E_γ regions. In contrast to the $E_{\rm CsI}$ distribution there are enhancements at low deposit energy, which must be due to the sampling effect that does not exist in the case of the CsI calorimeter. The detection inefficiency is obtained from the zero($E_{\rm Sand}$<1 MeV)-to-total ratio with a correction for the neutron detection efficiency which is obtained from a Poisson fit using the $m_{\rm LS}$ data in the runs for the sandwich calorimeter. The E_γ dependence of the detection inefficiency due to the photonuclear interaction is listed in Table 2 and is shown in Figure 23. The obtained inefficiency values are larger than those of the punch-through and the sampling effect due to the electromagnetic cascade shower process.

The detection inefficiency of the sandwich calorimeter is regarded to be dominated by the sampling effect caused by photonuclear interactions : the detection inefficiency arises when all of the charged particles produced by photonuclear interactions are absorbed in lead. Therefore, the converter (lead) should be thinner in order to reduce the detection inefficiency. For more understanding about the sandwich calorimeter a further experimental studies for the calorimeters having various converter thickness are necessary.

6 Summary

By analyzing the events in the low deposit-energy (tail) region for the CsI calorimeter of 30-cm long, the estimation of the punch-through using the EGS code is confirmed to be

correct.

The other source of the detection inefficiency, the photonuclear interaction, is identified by requiring neutron hits in the surrounding liquid-scintillation counters. The detection efficiency for neutrons of the liquid scintillation counters, which is the most important correction, is estimated from the Poisson distribution fit to the multiplicity distribution of the neutron hits. The obtained values of the efficiency are considerably large. This is due to the fact that a large number of neutrons (more than ten) are produced in a photonuclear interaction. The tail-to-total ratio shows the E_γ dependence consistent with that of the cross-section ratio between photonuclear interaction and electromagnetic cascade shower process obtained from previous experimental data. The obtained inefficiency due to the photonuclear interaction shows a monotonous decrease with energy and it is less than 1×10^{-5} above 300 MeV.

The result for the lead-scintillator sandwich counter indicates that the dominant process is the sampling effect after photonuclear interactions and that the detection inefficiency is as large as 1×10^{-4}. A further experimental study would be necessary to optimize the converter thickness.

The authors thank the operating crew of the INS-ES for their support during the present experiment.

References

[1] T. Inagaki et al., KEK Internal 96-13 (KEK-PS-E391 Proposal) (1996).

[2] T. Inagaki et al., Nucl. Instr. and Meth. **A359**, (1995) 478.

[3] W. R. Nelson, H. Hirayama and D. W. O. Rogers, SLAC Report 265 (1985).

[4] A. Leprêtre et al., Nucl. Phys. **A367**, (1981) 237; J. Ahrens et al., Nucl. Phys. **A251**, (1975) 479.

[5] S. Arai et al., Jpn. J. of App. Phys. **14**, (1975) 95.

[6] M. Mutoh, J. of Sci. of Hiroshima Univ. **51**, (1987) 187.

[7] P. Carlos et al., Nucl. Phys. **A431**, (1984) 573.

Photon Energy (MeV)	Ineff.(Punch Th.) ($\times 10^{-5}$)	Ineff.(Photonuclear) ($\times 10^{-5}$)
205	2.75 ± 0.37	1.11 ± 0.15
245	1.40 ± 0.26	1.12 ± 0.15
285	1.10 ± 0.23	0.71 ± 0.13
325	1.75 ± 0.30	0.81 ± 0.15
365	1.00 ± 0.22	0.39 ± 0.11
405	1.40 ± 0.26	0.37 ± 0.12
445	0.90 ± 0.21	0.21 ± 0.09
485	1.00 ± 0.22	< 0.13

Table 1. Detection inefficiencies of the CsI calorimeter.

Photon Energy (MeV)	Ineff.(EM-Cascade) ($\times 10^{-5}$)	Ineff.(Photonuclear) ($\times 10^{-4}$)
205	4.7 ± 1.0	1.15 ± 0.30
245	3.5 ± 0.5	1.72 ± 0.39
285	2.5 ± 0.4	1.49 ± 0.40
325	2.1 ± 0.4	1.62 ± 0.45
365	2.0 ± 0.3	2.32 ± 0.60
405	2.0 ± 0.3	1.22 ± 0.46
445	2.1 ± 0.3	0.99 ± 0.44
485	2.3 ± 0.4	1.13 ± 0.57

Table 2. Detection inefficiencies of the lead-scintillator sandwich calorimeter.

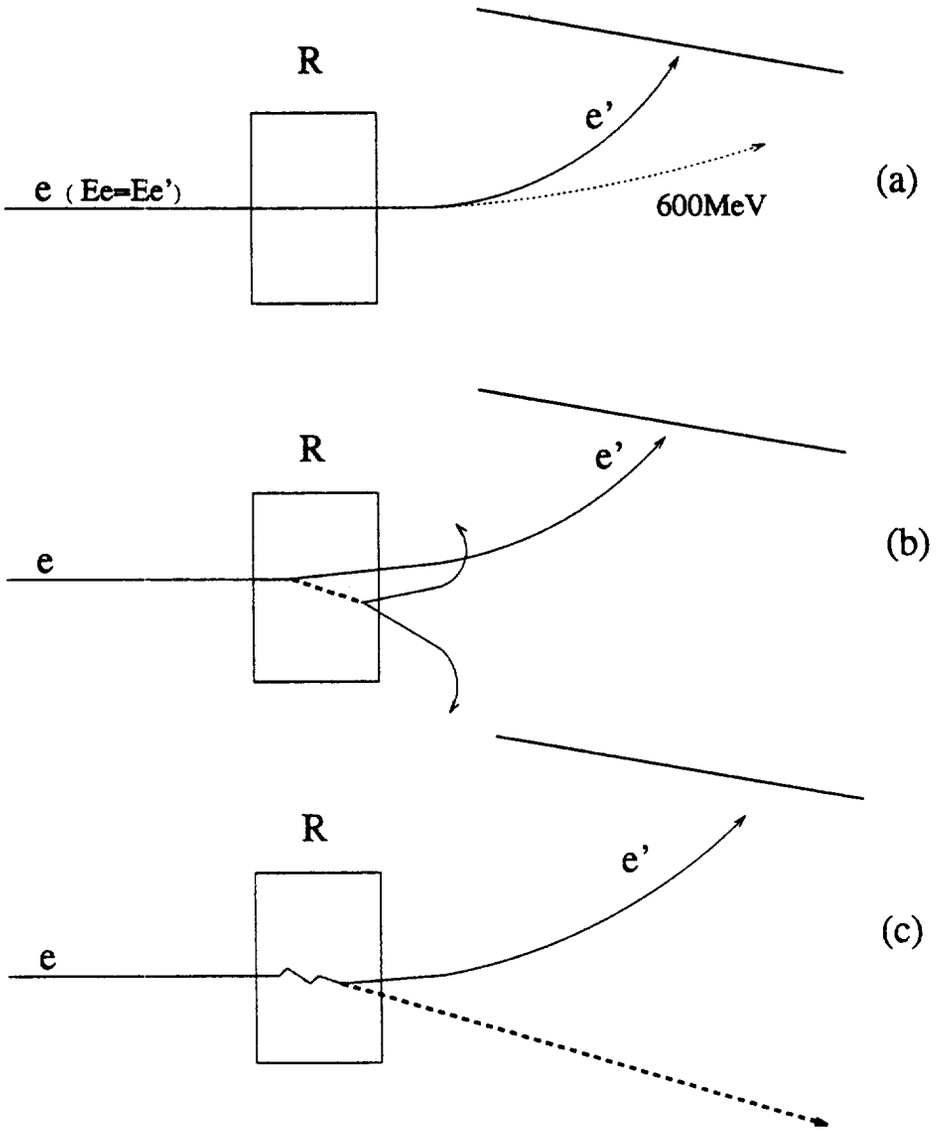

Figure 1: Processes to cause the miss tagging: (a) low-energy beam electrons, (b) two-step interactions in the radiator and (c) large-angle emission of photons. e, e' and R are the incident electron, the scattered one and the radiator, respectively.

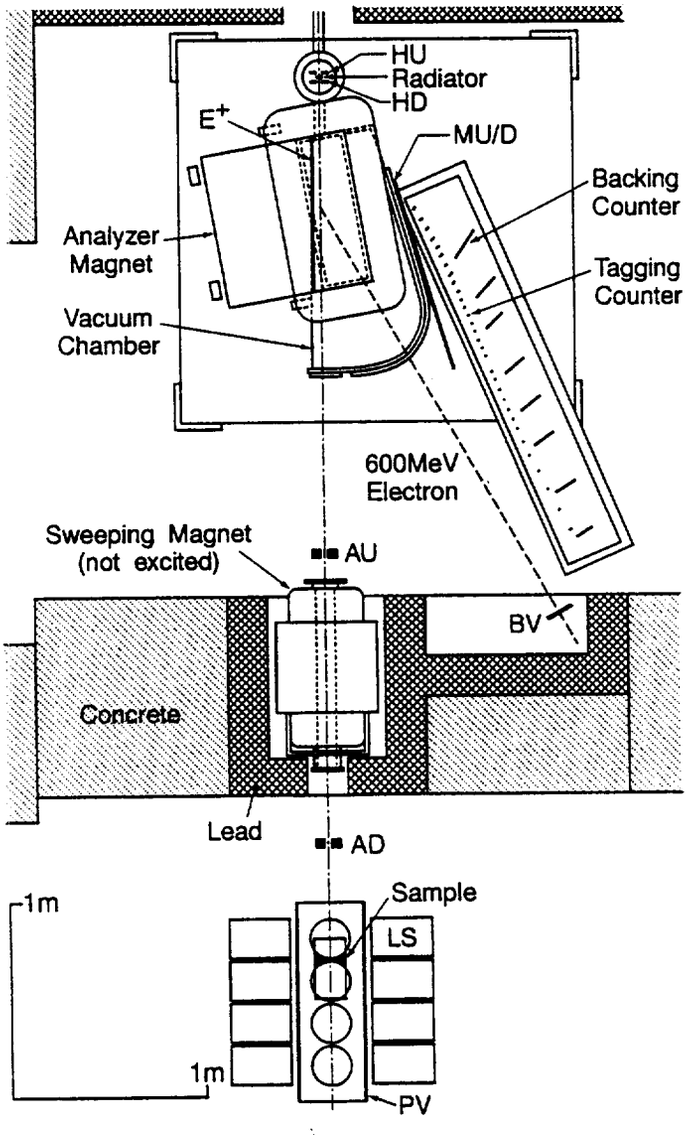

Figure 2: Plan-view of the experimental setup. The newly-installed veto-counters, HU/D, E^+, MU/D, BV and AU/D are described in the text.

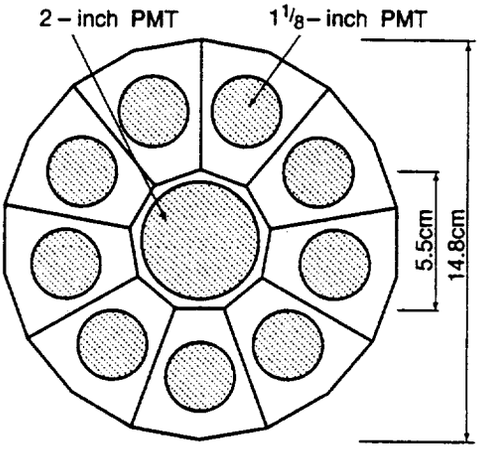

Figure 3: Front view of the CsI calorimeter.

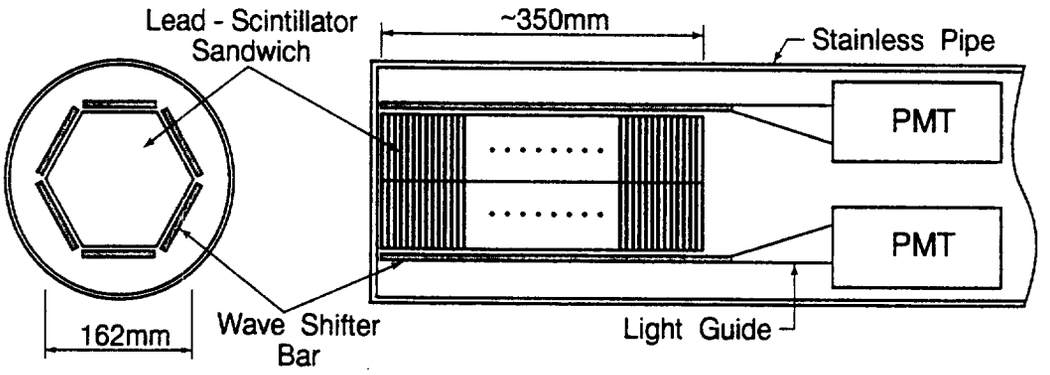

Figure 4: Lead-scintillator sandwich calorimeter.

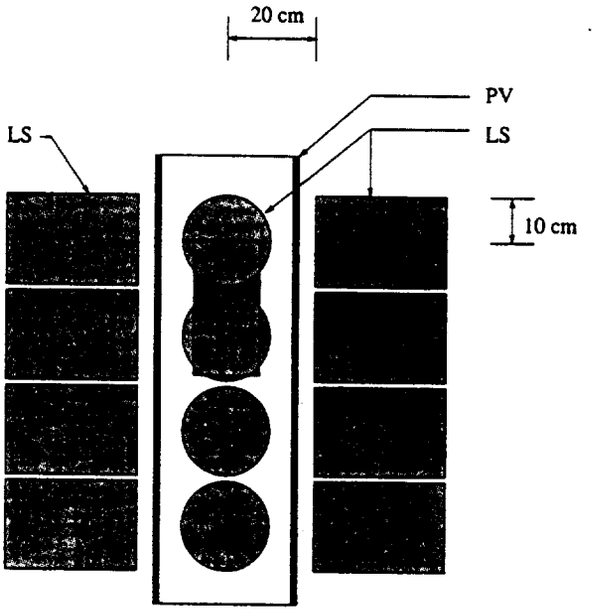

Plan View

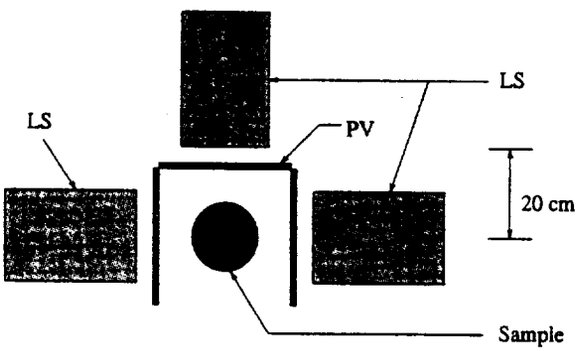

Front View

Figure 5: Setup around the sample calorimeter.

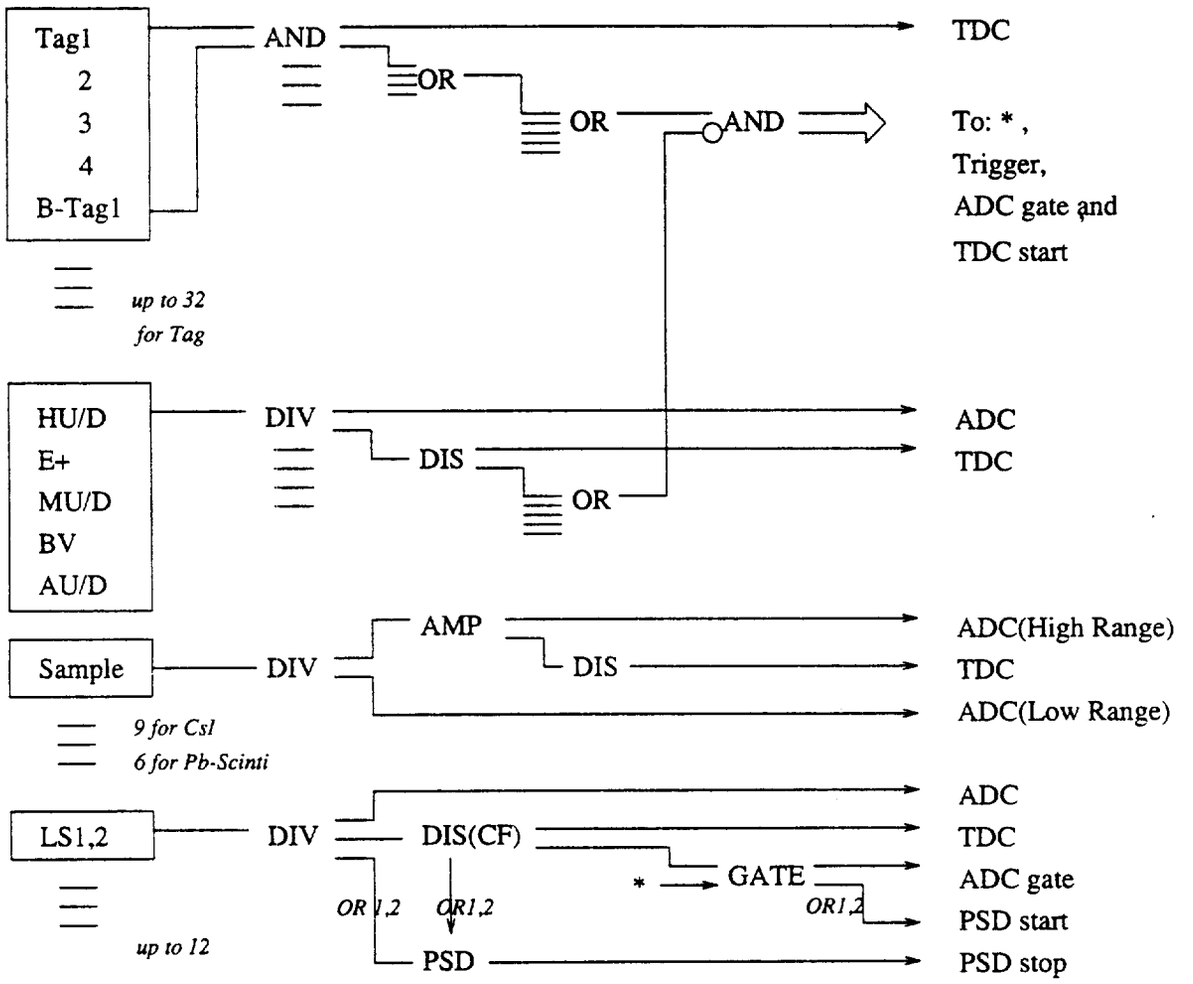

Figure 6: Electronics block diagram.

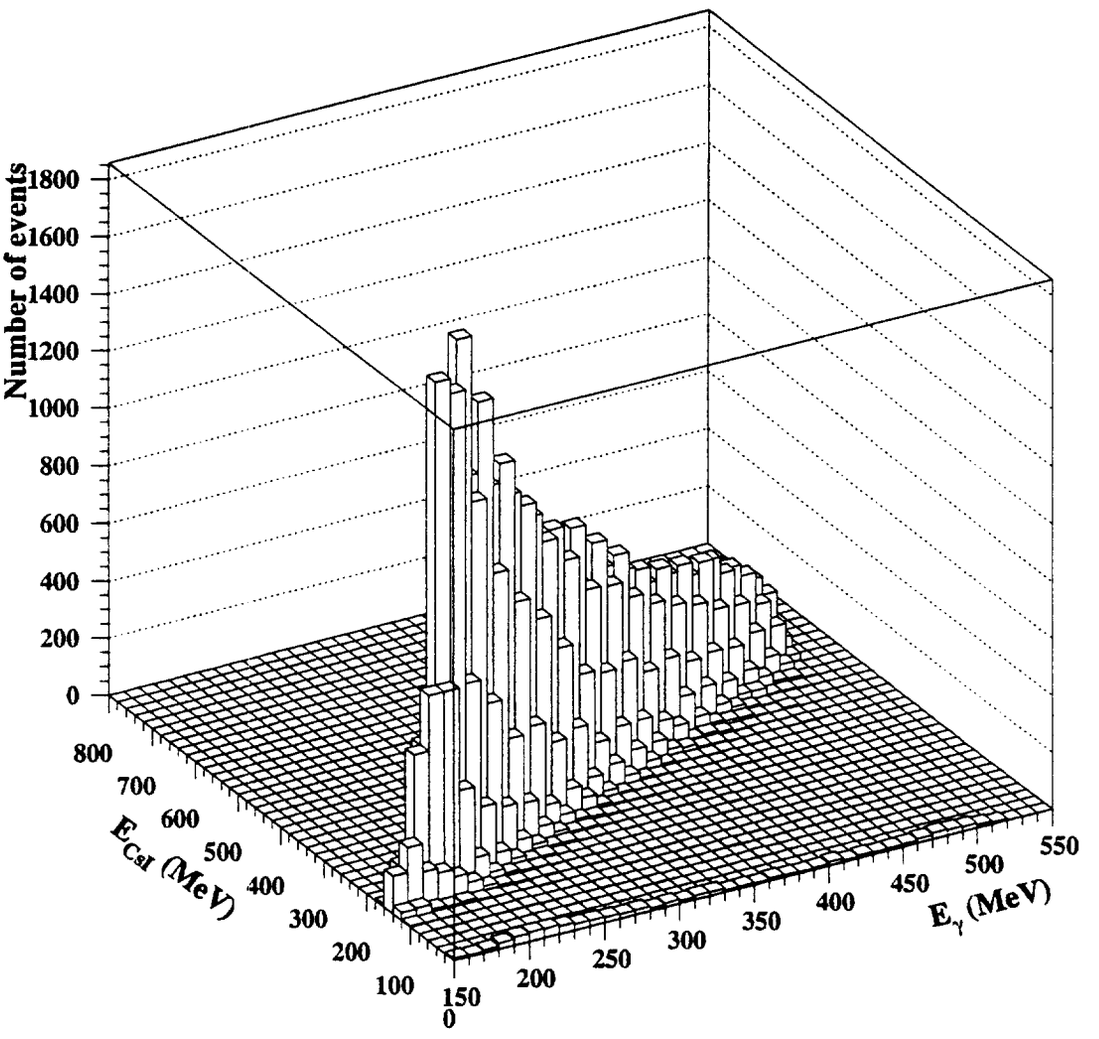

Figure 7: E_γ vs E_{CsI} correlation.

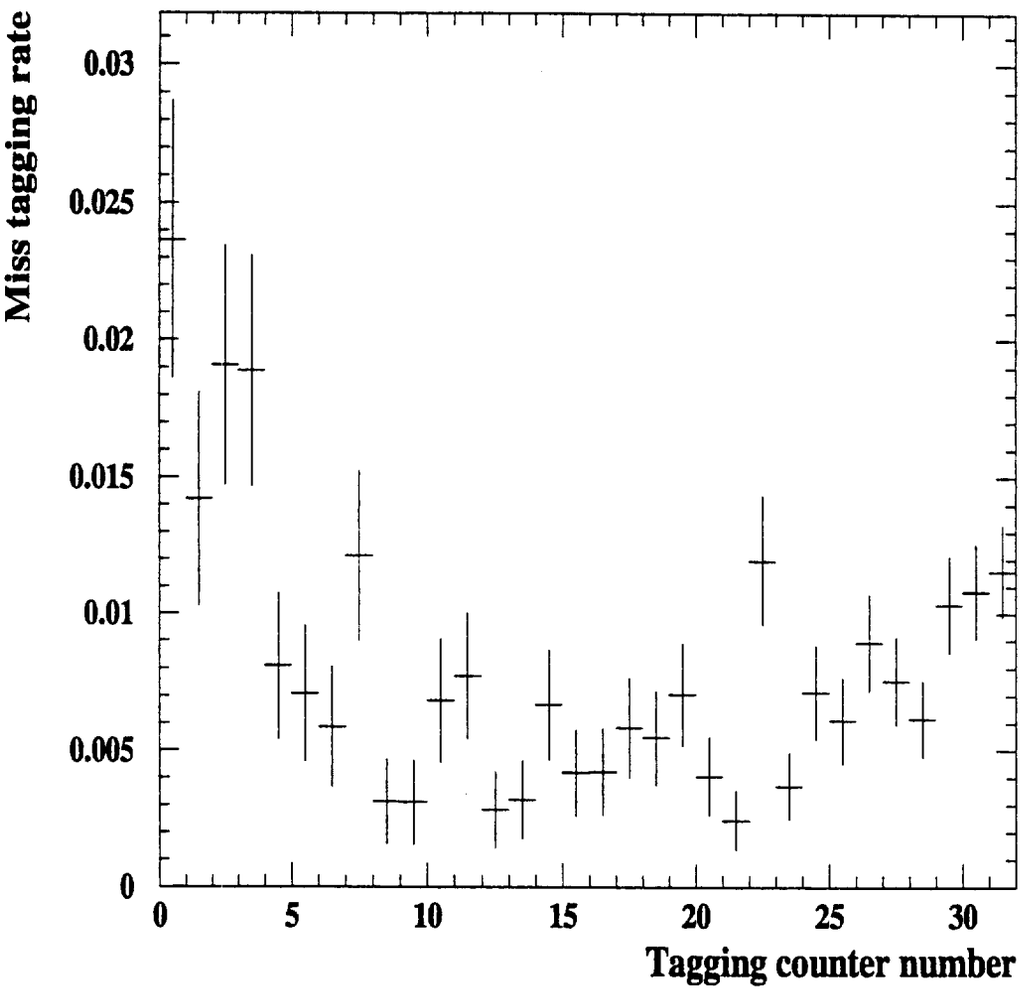

Figure 8: Tagging-counter-number dependence of the miss tagging rate.

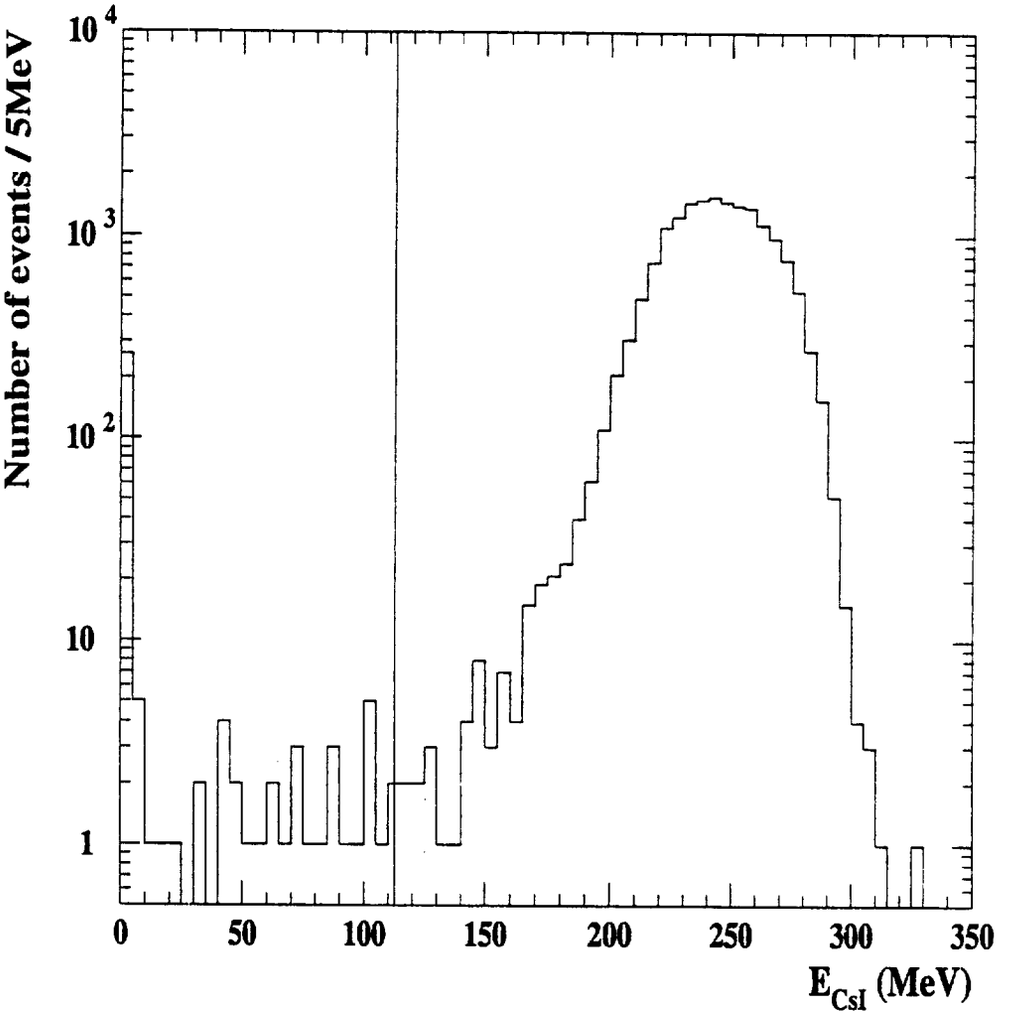

Figure 9: E_{CsI} distribution at E_γ=250±20 MeV. The line indicates the upper bound of the tail events for E_γ=250 MeV data.

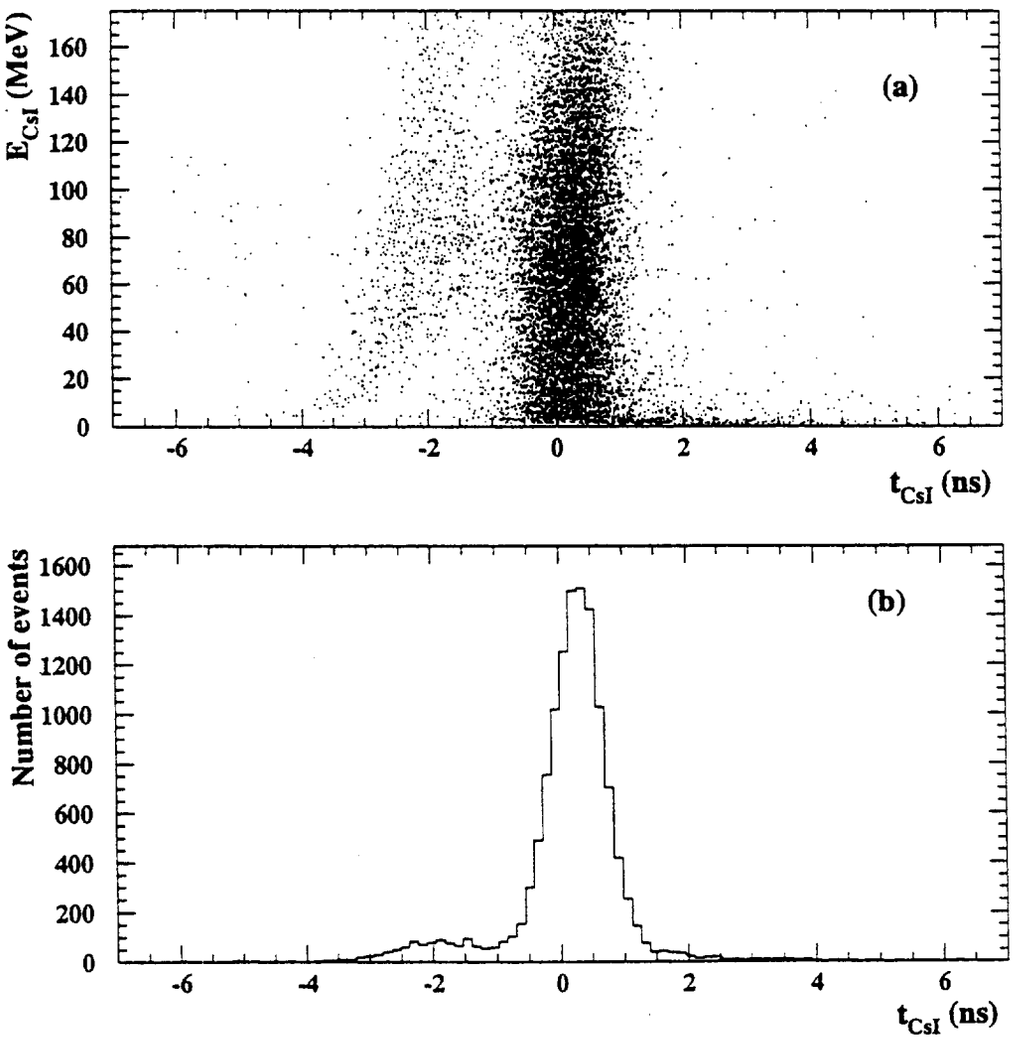

Figure 10: Time information of the CsI calorimeter signals (t_{CsI}) for the tail events: (a) a two-0 plot of t_{CsI} vs E_{CsI} and (b) its projected distribution on to the t_{CsI} axis.

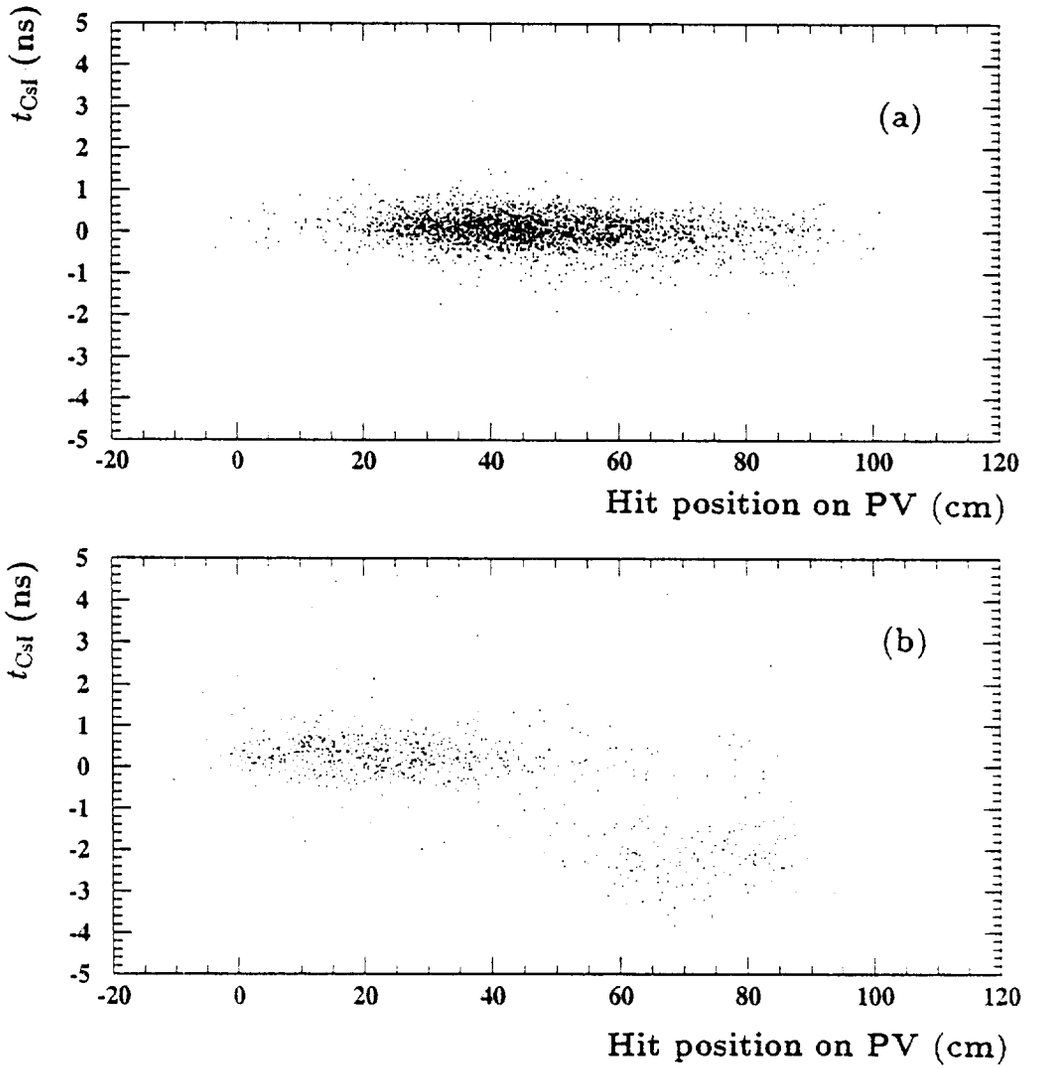

Figure 11: Correlations between t_{CsI} and a hit position on PV, (a) for all events including the peak region and (b) for the events in the tail region. The CsI calorimeter of 30-cm long is placed between 20-cm and 50-cm in the scale of abscissa. Two clusters are separated at t_{CsI}=-1 ns.

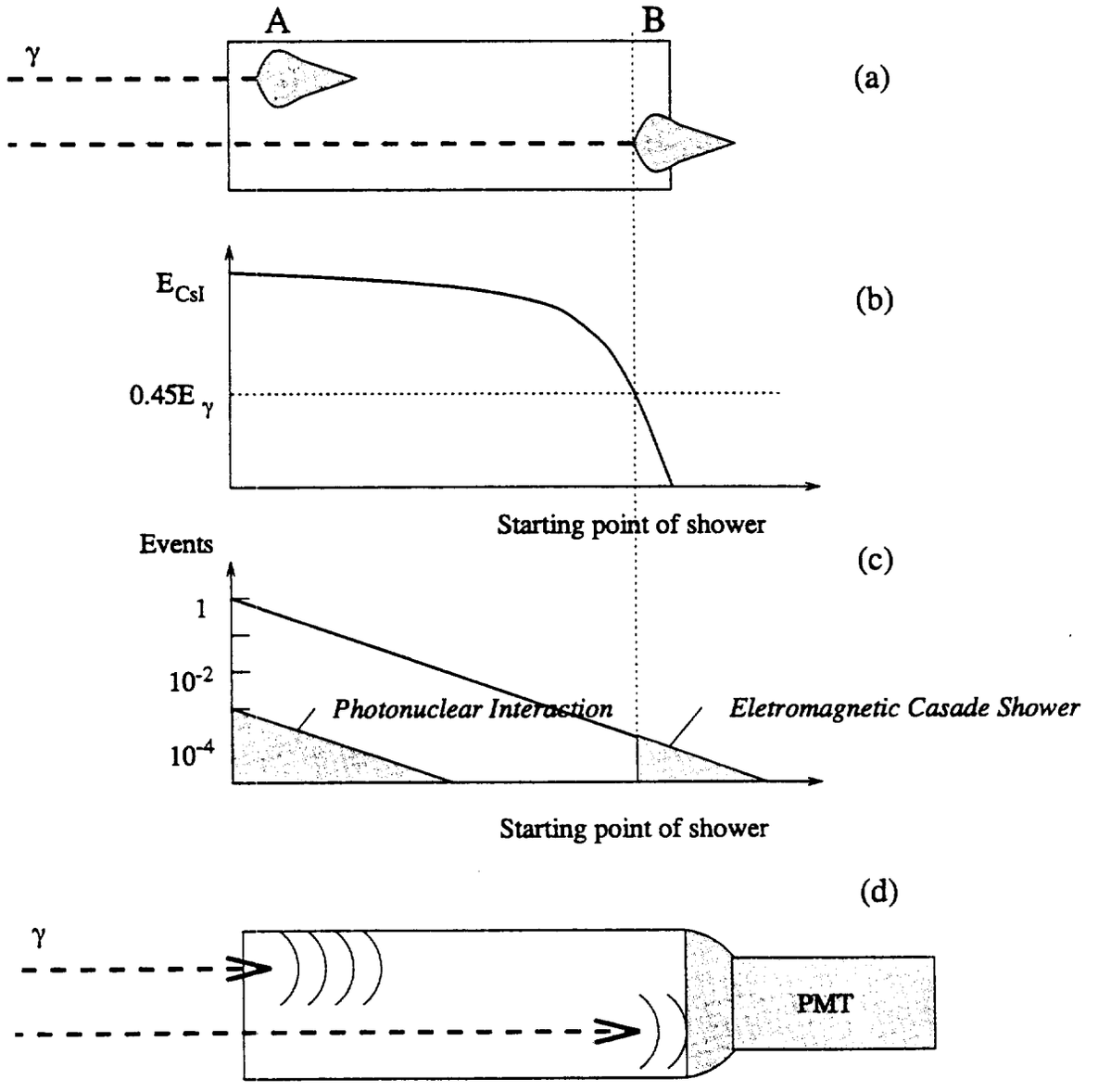

Figure 12: Explanation of the two-clusters in the tail region: (a) a general feature of the cascade showers whose starting points are shown by A (an ordinary point) and B (an very deep point), (b) a shower-start-point dependence of the deposit energy (E_{CsI}), (c) the attenuation of the incident photons (Two shaded areas correspond to the events remained in the tail region.), and (d) the behavior of the light propagation in the calorimeter.

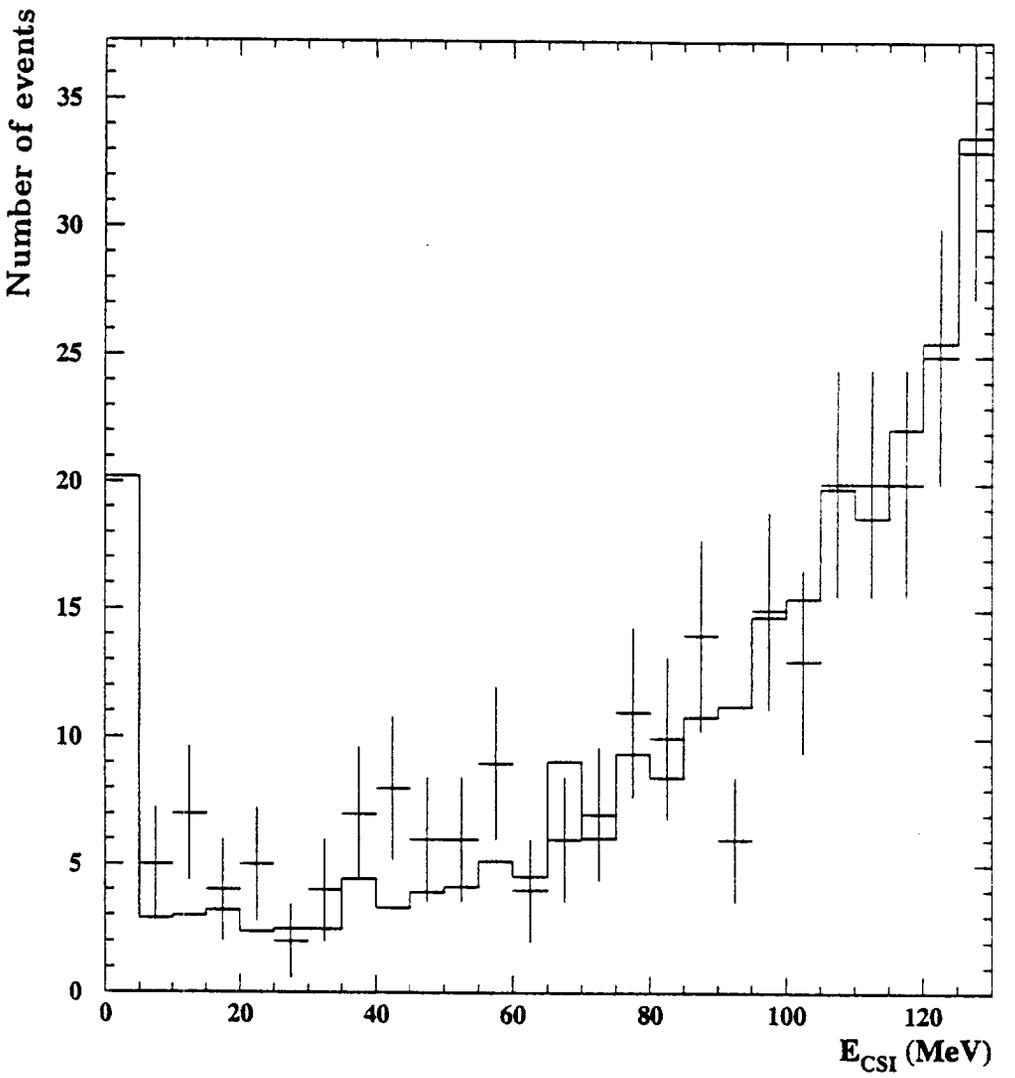

Figure 13: E_{CsI} distribution in the tail region: the data with error bars are for the events having early timings (-4ns<t_{CsI} <-1ns) and the histogram shows an EGS calculation.

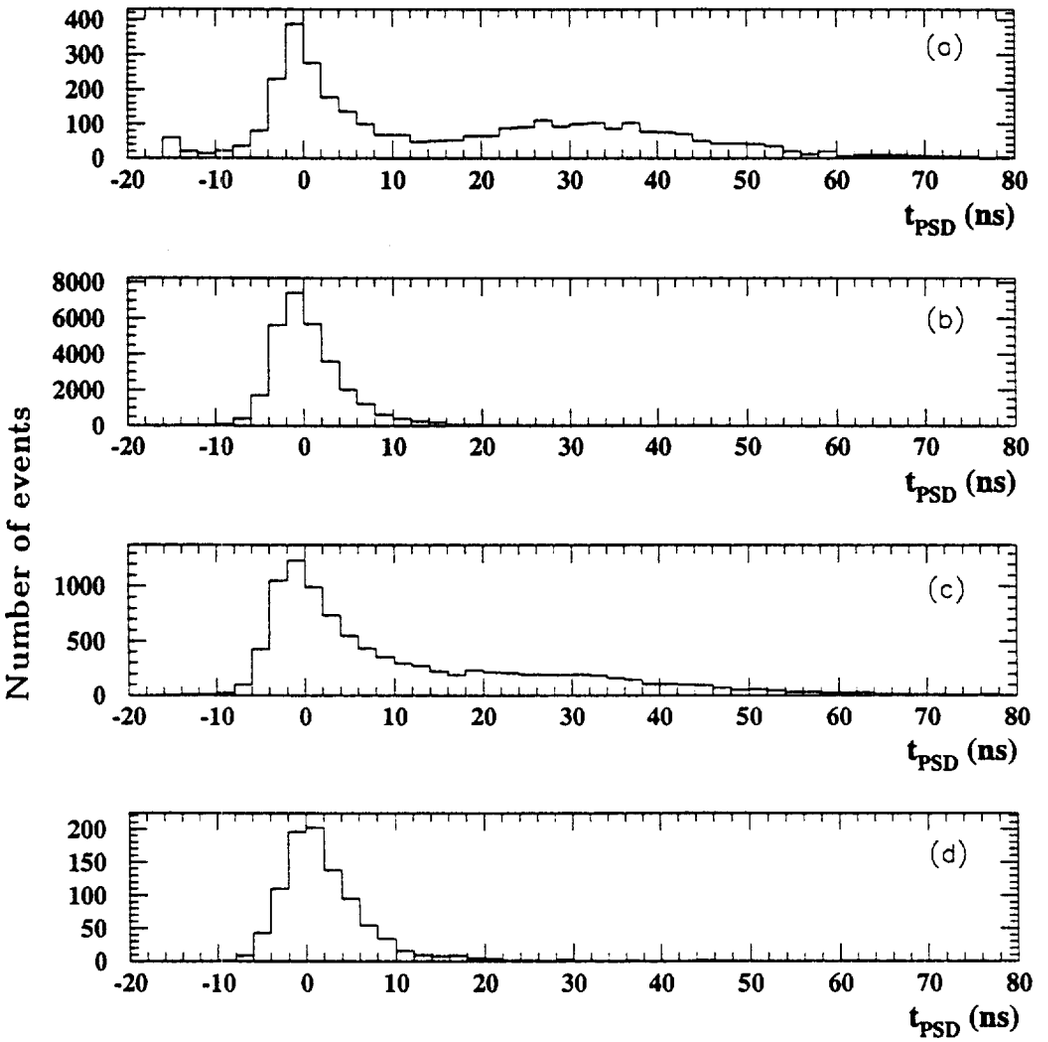

Figure 14: Time spectra measured with PSD for (a) the monitor data using an Am/Be source; the peak at $t_{PSD} \simeq 0$ corresponds to γ rays and the bump above 10 ns to neutrons, (b) the events in the peak region, (c) the tail region events with -1ns$<t_{CsI}<$2ns and (d) those with -4ns$<t_{CsI}<$-1ns.

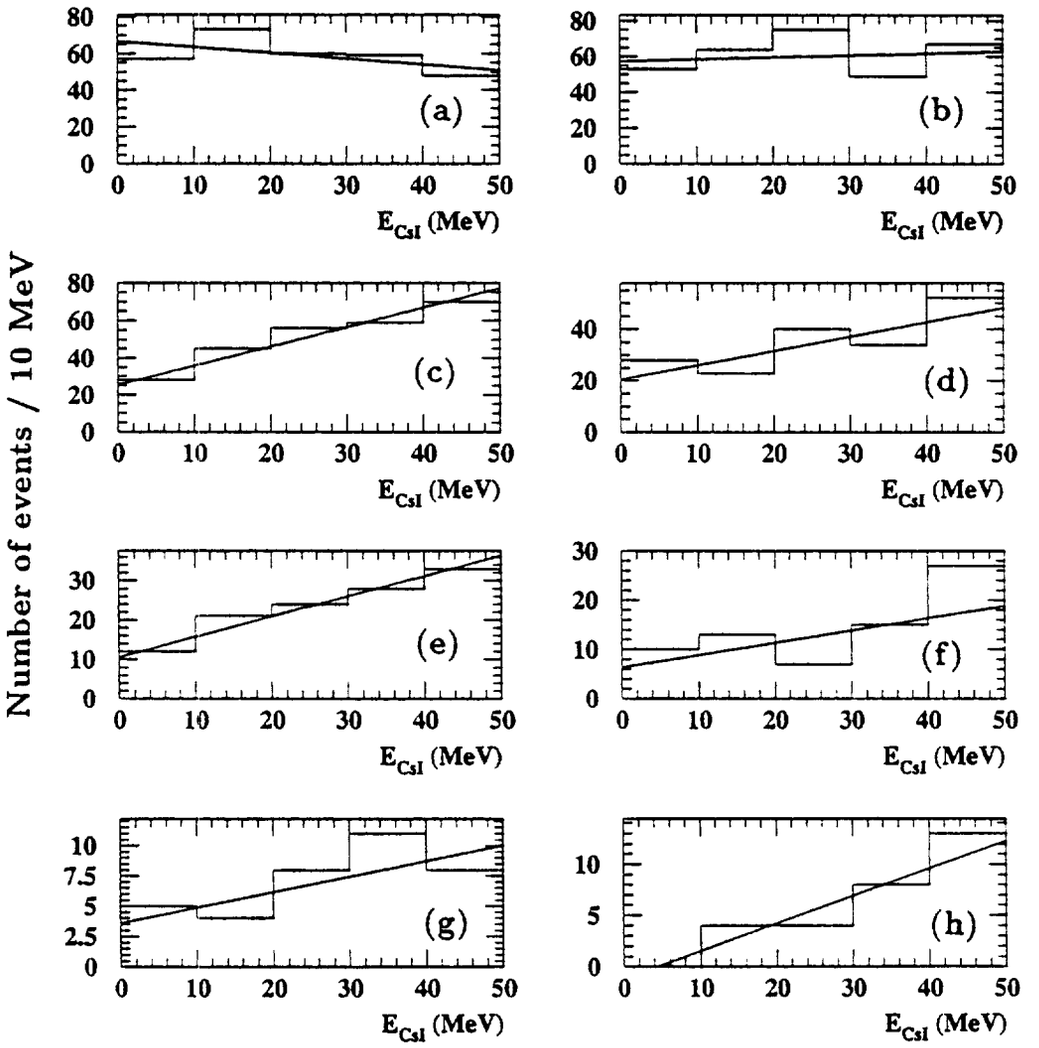

Figure 15: E_{CsI} distributions with the neutron-call in the various photon energy ranges (a)-(h): for E_γ of every 40 MeV bin from 185 MeV to 505 MeV. A straight line fit to the data is shown as an eye guide.

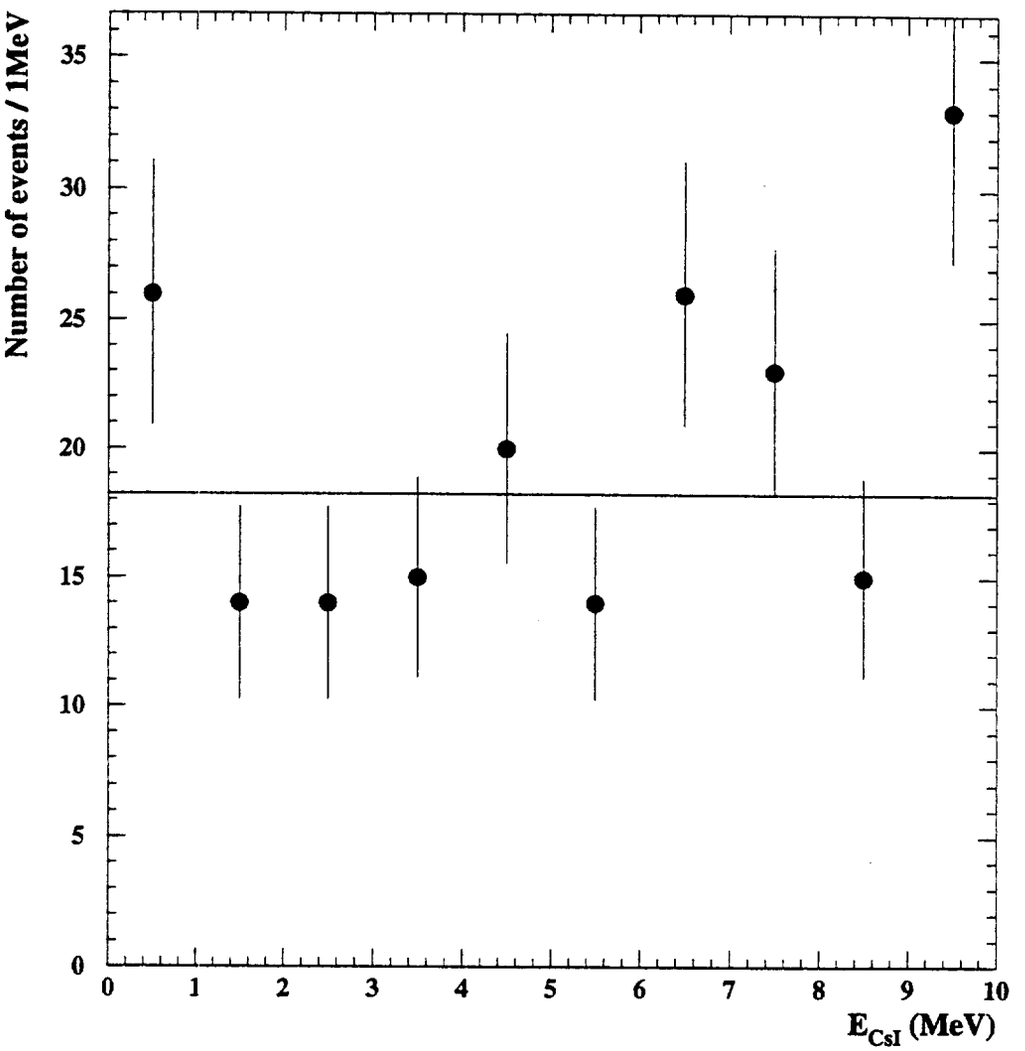

Figure 16: E_{CsI} distributions with the neutron-call for all E_γ events. The mean value is indicated by the solid line.

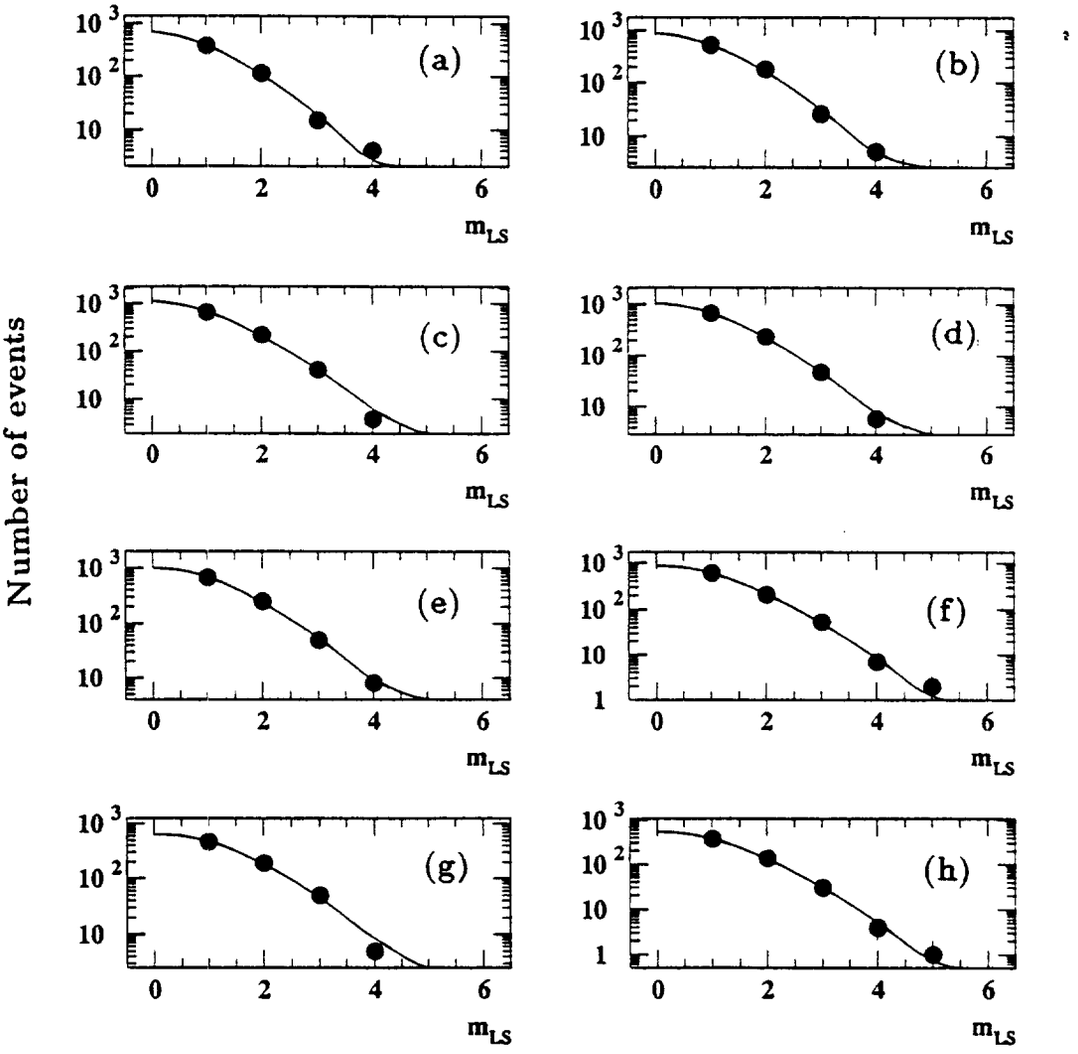

Figure 17: Multiplicity distributions of the liquid scintillation counters with neutron signal ($m_{\rm LS}$): (a)-(h) are those for every 40 MeV bin of E_γ from 185 MeV to 505 MeV. The curves are the Poisson distribution fit to the data of $m_{\rm LS}\geq 1$.

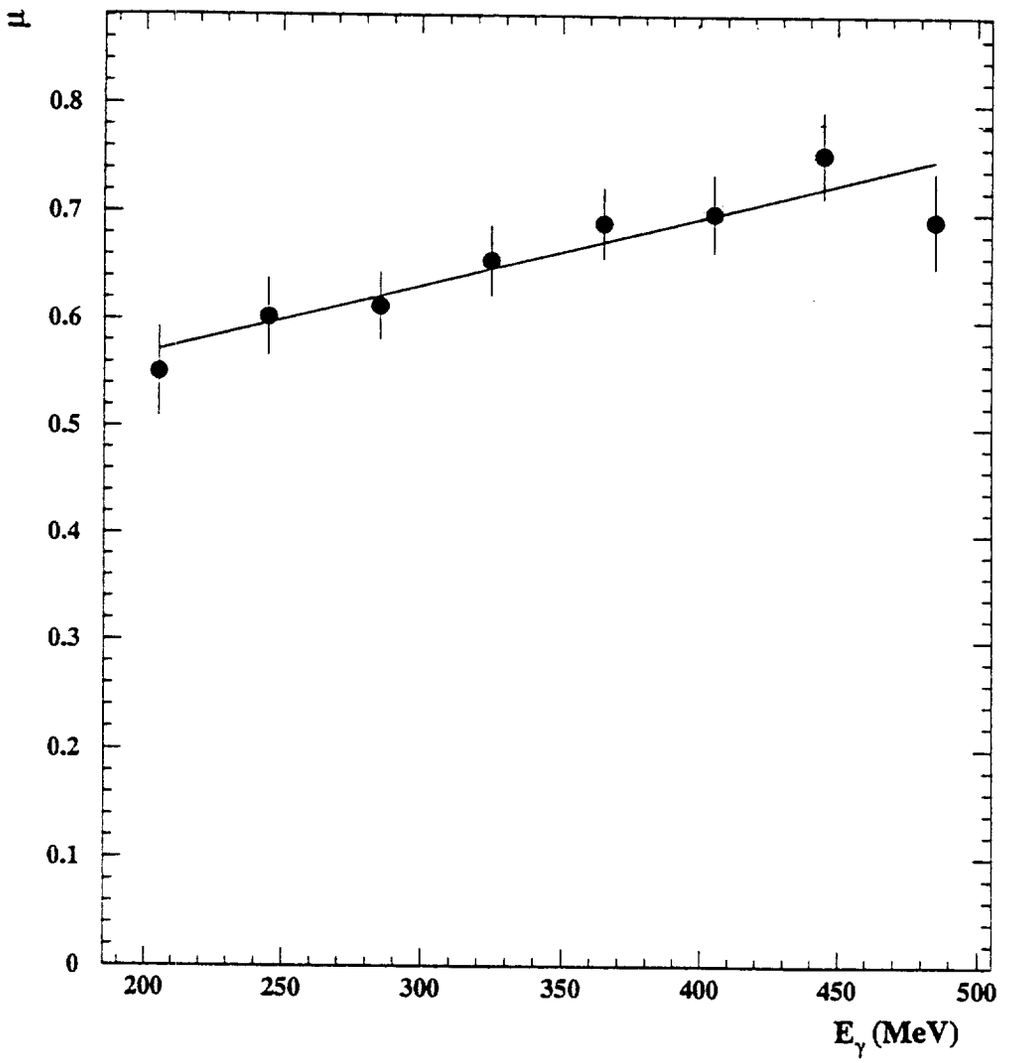

Figure 18: E_γ dependence of the mean value of the Poisson distribution, μ.

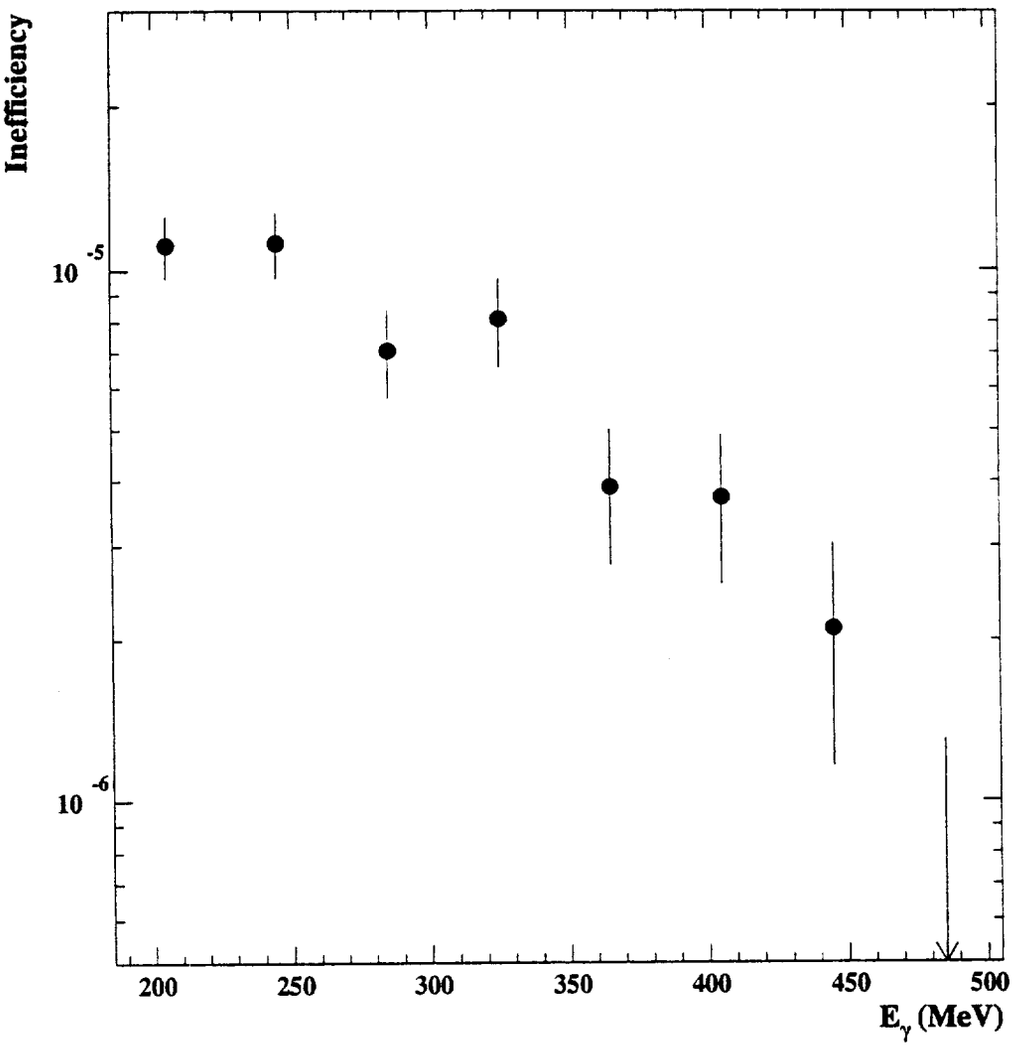

Figure 19: Detection inefficiencies of the CsI calorimeter due to the photonuclear interaction. The error includes the error of the neutron detection efficiency as well as the statistical fluctuation of the E_{CsI}<1MeV events. The upper limit at the highest energy point is given as the value with a 90 % confidence level.

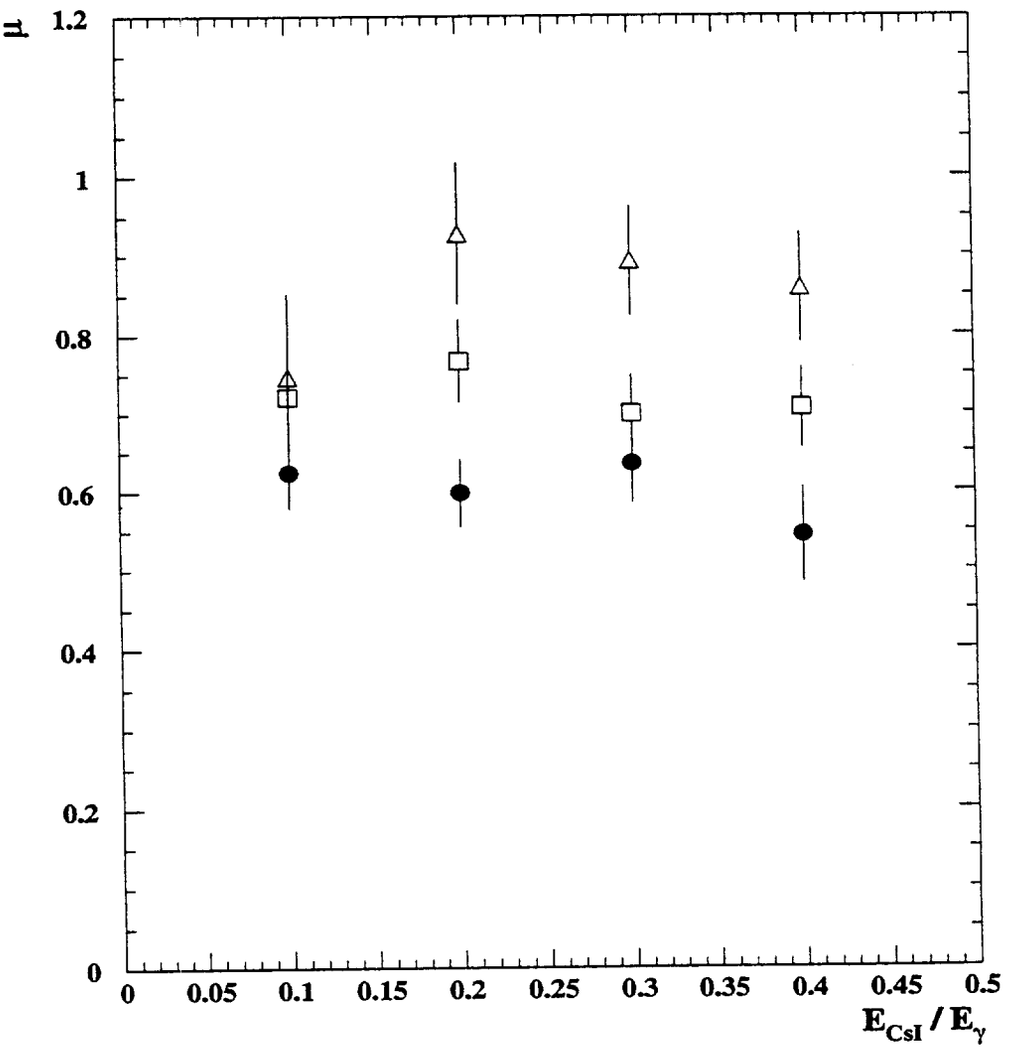

Figure 20: The variation of μ for different E_γ and $E_{\rm CsI}/E_\gamma$ regions. The $\bullet$, $\Box$ and $\triangle$ are the μ values obtained in the regions E_γ =250$\pm$50 MeV, 350$\pm$50 MeV and 450$\pm$50 MeV, respectively, and the $E_{\rm CsI}/E_\gamma$ region is $\pm$0.05

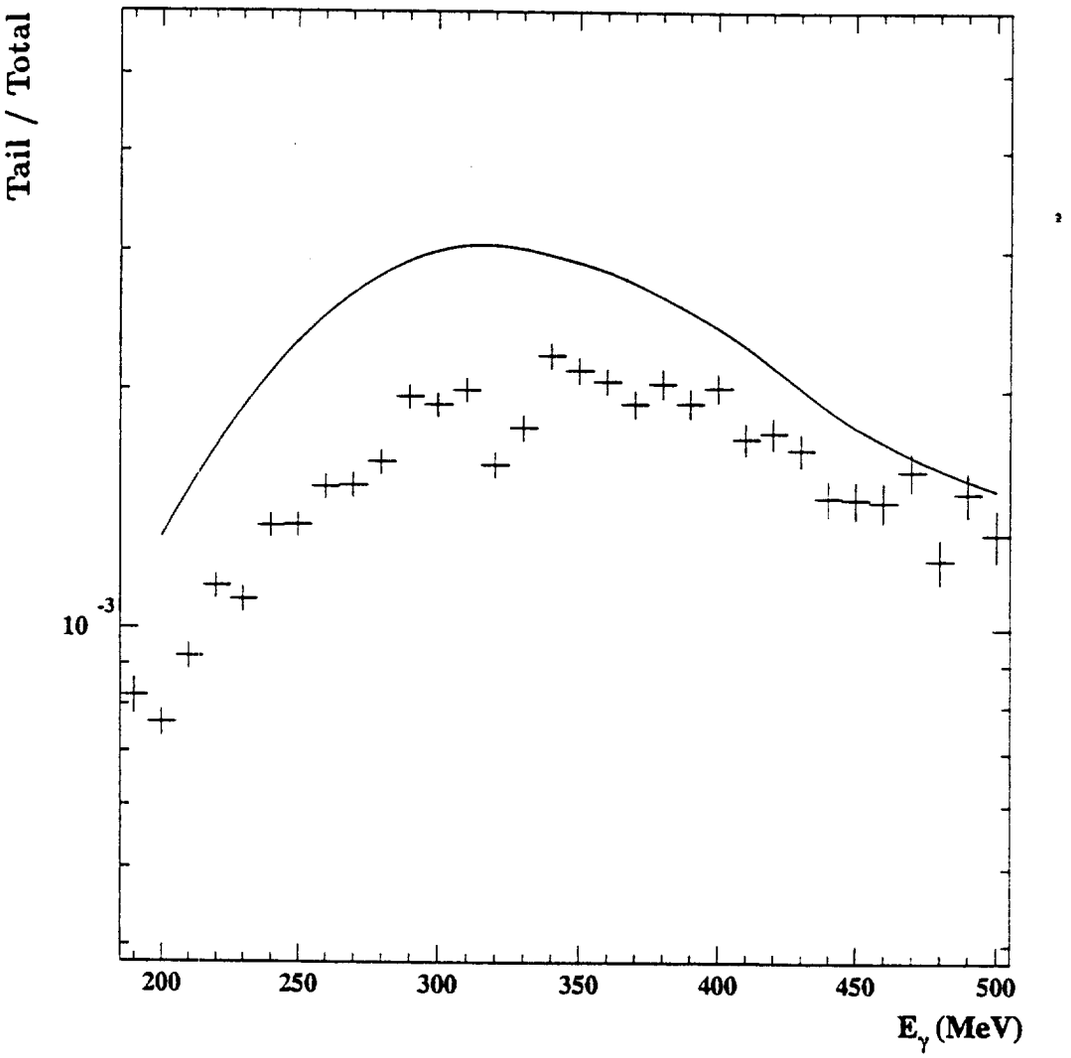

Figure 21: Photon-energy dependence of the tail-to-total ratio, where the tail events are those with neutron signals and the ratio corrected for the neutron detection efficiency. The curve is calculated from the ratio of the cross section between the photonuclear and electromagnetic interactions.

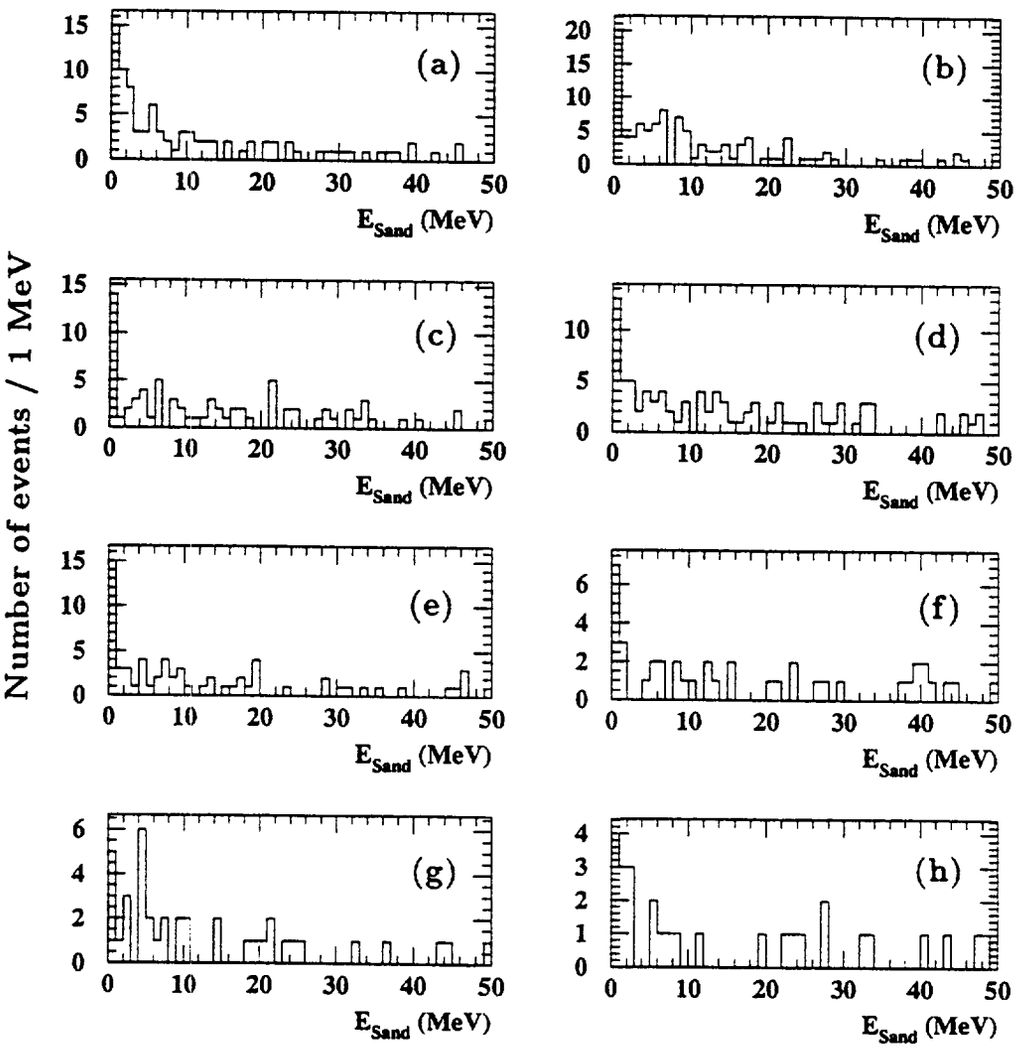

Figure 22: E_{Sand} distributions with the neutron-call for the data in every 40 MeV bin of E_γ from 185 MeV to 505 MeV ((a)-(h)).

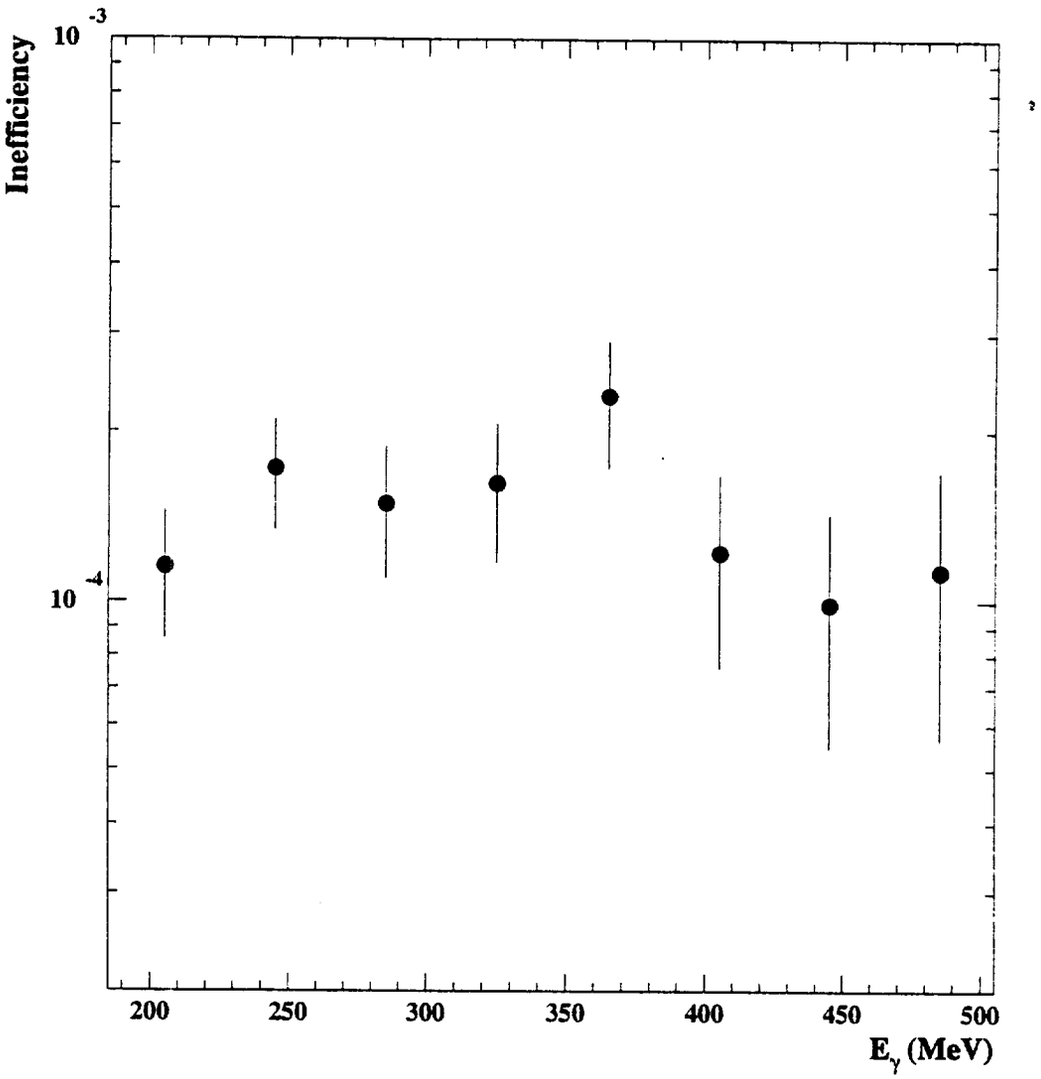

Figure 23: Detection inefficiency of the lead-scintillator sandwich calorimeter due to the photonuclear interaction. The error comes from the uncertainty in the neutron detection efficiency as well as the statistical fluctuation of the E_{Sand}<1MeV events.